



Deposited via The University of Leeds.

White Rose Research Online URL for this paper:

<https://eprints.whiterose.ac.uk/id/eprint/126633/>

Version: Accepted Version

---

**Article:**

Naik, B, Khatua, KK, Wright, N et al. (2018) Numerical modeling of converging compound channel flow. *ISH Journal of Hydraulic Engineering*, 24 (3). pp. 285-297. ISSN: 0971-5010

<https://doi.org/10.1080/09715010.2017.1369180>

---

(c) 2017, Indian Society for Hydraulics. This is an Accepted Manuscript of an article published by Taylor & Francis in the *ISH Journal of Hydraulic Engineering* on 20 September 2017, available online: <https://doi.org/10.1080/09715010.2017.1369180>

**Reuse**

Items deposited in White Rose Research Online are protected by copyright, with all rights reserved unless indicated otherwise. They may be downloaded and/or printed for private study, or other acts as permitted by national copyright laws. The publisher or other rights holders may allow further reproduction and re-use of the full text version. This is indicated by the licence information on the White Rose Research Online record for the item.

**Takedown**

If you consider content in White Rose Research Online to be in breach of UK law, please notify us by emailing [eprints@whiterose.ac.uk](mailto:eprints@whiterose.ac.uk) including the URL of the record and the reason for the withdrawal request.

# Numerical modeling of Converging Compound Channel Flow

B. Naik<sup>1</sup>, K.K.Khatua<sup>2</sup> N. G. Wright<sup>3</sup>, and A. Sleight<sup>4</sup> P. Singh<sup>5</sup>

1 Ph. D. Research Scholar, Department of Civil Engineering, National Institute of Technology Rourkela, India. Email:banditanaik1982@gmail.com

2 Associate Professor, Department of Civil Engineering, National Institute of Technology Rourkela, India. Email: kkkhatua@yahoo.com

3 Professor of Water and Environmental Engineering, University of Leeds, School of Civil Engineering, UK. Email: n.g.wright@leeds.ac.uk

4 Professor, Department of Water and Environmental Engineering, University of Leeds, School of Civil Engineering, UK. Email: p.a.sleight@leeds.ac.uk

5 M.Tech Scholar, Department of Civil Engineering, National Institute of Technology Rourkela, India. Email:prateek.k.singh1992@gmail.com

## Abstract

This paper presents numerical analysis for prediction of depth-averaged velocity distribution of compound channels with converging flood plains. Firstly, a 3D Computational Fluid Dynamics (CFD) model is used to establish the basic database under various working conditions. Numerical simulation in two phases is performed using the ANSYS-Fluent software.  $k-\omega$  turbulence model is executed to solve the basic governing equations. The results have been compared with high quality flume measurements obtained from different converging compound channels in order to investigate the numerical accuracy. Then ANN (Artificial Neural Network) are trained based on the Back Propagation Neural Network (BPNN) technique for depth-averaged velocity prediction in different converging sections and these test results are compared with each other and with actual data. The study has focused on the ability of the software to correctly predict the complex flow phenomena that occur in channel flows.

**Keywords:** *compound channel, stage discharge, Prismatic, non-prismatic, ANN, ANSYS*

## 1 INTRODUCTION

Distribution of depth-averaged velocity is important aspect in river hydraulics and engineering problems in order to give a basic understanding of the resistance relationship, to understand the mechanisms of sediment transport and to design sustainable channels etc. Due to continuous settlement of people near the riverbank and due to natural causes, the channel with floodplain cross-sections behaves as converging type non-prismatic compound channels. An improper estimation of floods in these regions, will lead to an increase in the loss of life and property. A number of authors [1-8] has investigated the depth-averaged velocity distribution and flow resistance in prismatic compound cross-sections. These models are not appropriate to predictions in compound channels with converging flood plain because of non-uniform flow occurs from section to section. Therefore, there is a need to evaluate the depth-averaged velocity in the main channel and floodplain at various locations of a converging compound channel. Converging channel flows, being highly complicated, are a matter of recent and continued research. For a

47 better understanding of the structure of turbulent flow in converging compound channels, it is  
48 necessary to undertake detailed measurements. Because of the difficulty in obtaining sufficiently  
49 accurate and comprehensive field measurements of velocity and shear stress in converging  
50 compound channels under non-uniform flow conditions, considerable reliance must still be  
51 placed on well focused laboratory investigations under steady flow conditions to provide the  
52 information concerning the details of the flow structures and lateral momentum transfer.  
53 Attention must be paid to the fact that physical models are very expensive, especially when a  
54 large number of influencing parameters have to be studied. Sometimes, it is impossible to  
55 construct a physical model for certain prototypes. Therefore, there is urgent need for economic  
56 mathematical prediction models. In past a lot of experimental research has been done on  
57 prismatic compound channel flows but relatively less usage has been made of numerical  
58 techniques on non-prismatic compound sections. After the development of powerful computers  
59 and sophisticated CFD (Computational Fluid Dynamics) techniques, much research is now being  
60 conducted using these techniques in different research areas. This is not only due to economy  
61 and less time required with CFD methodology but also due to the fact that through CFD one can  
62 cover those aspects of flow behavior which are very difficult to observe through  
63 experimentation. In recent years, numerical modeling of open channel flows has successfully  
64 reproduced experimental results. Computational fluid dynamics (CFD) has been used to model  
65 open channel flows ranging from main channels to flood plains. Simulations have been  
66 performed by Krishnappan & Lau (1986), Kawahara & Tamai (1988) and Cokljat (1993). CFD  
67 has also been used to model flow features in natural rivers by Sinha et al. (1998), Lane et al.  
68 (1999), and Morvan (2001). Hodkinson (1996, 1998) was one of the first to present results using  
69 a commercial CFD. In this case FLUENT was used to predict the 3D flow structure in a 90-  
70 degree bend on the River Dean in Cheshire. Pan & Banerjee (1995), Hodges & Street (1999),  
71 and Nakayama & Yokojima (2002) studied free surface fluctuations in open channel flow by  
72 employing the LES method. Hsu *et al.* (2000) have reported the existence of the inner secondary  
73 currents in the rectangular open-channels, which occur at the junction of the free surface and  
74 sidewall. Knight *et al.* (2005) applied state-of-the-art CFD software to explore the physics within  
75 open-channel flows. In their research work they applied three different turbulent models, namely  
76 the  $k-\epsilon$ , Reynolds Stress model by Speziale, Sarkar and Gatski (SSG) by Speziale *et al.* (1991)  
77 and Reynolds Stress  $\omega$  or SMC- $\omega$  (implemented in ANSYS-CFX) models to trapezoidal channel.  
78 Thomas and Williams (1995a) and Cater and Williams (2008) simulated an asymmetric  
79 rectangular compound channel using LES for a relative depth of  $\beta = 0.5$ . They have predicted  
80 mean stream wise velocity distribution, secondary currents, bed shear stress distribution,  
81 turbulence intensities, TKE, and calculated lateral distribution of apparent shear stress. Gandhi et  
82 al. (2010) determined the velocity profiles in two directions under different real flow field  
83 conditions and also investigated the effects of bed slope, upstream bend and a convergence /  
84 divergence of channel width. Kara *et al.* (2012) compared the depth-averaged stream wise  
85 velocities obtained by LES with calculated by analytical solution of Shiono and Knight Method  
86 (SKM), and concluded that the analytical approach to their problem requires calibration of the  
87 lateral eddy viscosity coefficient,  $\lambda$ , and the secondary current parameter,  $\Gamma$ . Xie *et al.* (2013)  
88 used LES to simulate asymmetric rectangular compound channel. In this study the distributions  
89 of the mean velocity and secondary flows, boundary shear stress, turbulence intensities, TKE and  
90 Reynolds stresses were in a good agreement with the experimental data. Filonovich (2015) used  
91 ANSYS-CFX package to allow the simulation of uniform flows in straight asymmetric

92 trapezoidal and rectangular compound channels with several different RANS turbulence closure  
93 models.

94

95 In the last decade machine-learning methods were the subject of many researches in engineering  
96 problems and also in water resources engineering (Cheng et al., 2002; Lin et al., 2006;  
97 Muzzammil, 2008; Wang et al., 2009; Wu et al. 2009; Ghosh et al., 2010; Safikhani et al.,  
98 2011). Bilgil and Altun (2008) predicted friction factor in smooth open channel flow using ANN.  
99 Sahu et al. (2011) proposed an artificial neural network model for accurate estimation of  
100 discharge in compound channel flume and Moharana and Khatua (2014) studied the flow  
101 resistance in meandering compound channels by using ANFIS. Abdeen (2008) adopted an ANN  
102 technique to simulate the impacts of vegetation density, flow discharge and the operation of  
103 distributaries on the water surface profile of open channels. Yuhong and Wenxin (2009) studied  
104 the application of ANN for prediction of friction factor of open channel flows. The ANN  
105 technique has also been successfully applied to compound open channel flow for the prediction  
106 of the hydraulics characteristics, such as integrated discharge and stage-discharge relations  
107 (Bhattacharya & Solomatine 2005; Jain 2008; Unal et al. 2010; Sahu et al.2011)

108

109 In the first part of this paper, 3D numerical simulations of flow field with two phases (water &  
110 air) are carried out with the software ANSYS FLUENT to study the variation of velocity profiles  
111 in different converging sections of a compound channel. In multiphase fluid flow, a phase is  
112 described as a particular class of material that has a certain inertial response and interaction with  
113 the fluid flow and the potential field in which it is immersed. Currently there are two approaches  
114 for the numerical calculation of multiphase flows: The Euler-Lagrange approach and the Euler-  
115 Euler approach. Even though air is considered as a secondary material we have taken it in  
116 analysis to give it more real time analogy, by compromising over the computational time.

117 In order to solve turbulence equations, the  $k-\omega$  model is used since more accurate near wall  
118 treatment with automatic switch from wall function to a low Reynolds number formulation based  
119 on grid spacing. Numerical results are verified using experimental data obtained in an  
120 experimental analysis in the Hydraulics and Fluid Mechanics Laboratory of the Civil  
121 Engineering Department of NIT, Rourkela. This study shows that the numerical model results  
122 have good agreement with experimental ones. There are always some limitations in experimental  
123 studies and obtaining experimental data in every point of a channel is not easy. Also after doing  
124 an experimental test and obtaining the velocity in the desired point, measuring the velocity in  
125 other points needs to do the experimental test again. Artificial intelligence is evaluated here as a  
126 solution to this problem. By training an ANN based on experimental data of the points that are  
127 available, the ANN assists investigators in calculating the velocity at other points of the channel  
128 with good accuracy. This paper employs ANN for the prediction of depth average velocity of  
129 converging compound channel, after using the computational fluid dynamics (CFD) technique to  
130 establish the basic database under various working conditions. Quite a few model available for  
131 prediction of depth average velocity usually under performs when the meagre datasets are used  
132 for estimation. Generally, this happens while predicting the depth average velocity for a wide  
133 range of hydraulic conditions and geometries of compound channel. To alleviate the above  
134 problem, a robust prediction strategy based on an ANN has been proposed. It is demonstrated  
135 that the ANN model is quite capable of predicting a depth average velocity with reasonable  
136 accuracy for a wide range of hydraulic conditions.

137

138 **2 EXPERIMENTAL WORKS**

139 Experiments have been conducted at the Hydraulics and Fluid mechanics Laboratory of Civil  
140 Engineering Department of National Institute of Technology, Rourkela, India. Three sets of non-  
141 prismatic compound channels with varying cross section were built inside a concrete flume with  
142 Perspex sheet measuring 15m long  $\times$  0.90m width  $\times$  0.5m depth. The width ratio ( $\alpha$  = flood plain  
143 width (B)/main channel width (b)) of the channel was 1.8 and the aspect ratio ( $\delta$  = main channel  
144 width (b)/main channel depth (h)) was 5. Keeping the geometry constant, the converging angles  
145 of the channels were varied as  $12.38^\circ$ ,  $9^\circ$  and  $5^\circ$  respectively. Converging length of the channels  
146 fabricated were found to be 0.84m, 1.26m and 2.28m respectively. Longitudinal bed slope of the  
147 channel was measured to be 0.0011, satisfying subcritical flow conditions at all the sections of  
148 the non-prismatic compound channels. Roughness of both floodplain and main channel were  
149 kept smooth with the Manning's  $n$  0.011 determined from the inbank experimental runs in the  
150 channel. The flow conditions in all sections were turbulent. A re-circulating system of water  
151 supply was established with pumping of water from the large underground sump located in the  
152 laboratory to an overhead tank from where water flows under gravity to the experimental  
153 channels. Adjustable vertical gates along with flow strengtheners were provided in the upstream  
154 section sufficiently ahead of rectangular notch to reduce turbulence and velocity of approach in  
155 the flow near the notch section. An adjustable tailgate at the downstream end of the flume helps  
156 to maintain uniform flow over the test reach. Water from the channel was collected in a  
157 volumetric tank of fixed area that helps to measure the discharge rate by the time rise method.  
158 From the volumetric tank water runs back to the underground sump by the valve arrangement.  
159 For present work the experimental data Rezaei (2006) have been used. Rezaei (2006) have also  
160 used converging compound channels of angles  $11.31^\circ$ ,  $3.81^\circ$ ,  $1.91^\circ$  giving the same subcritical  
161 flow and smooth surfaces. They have found the depth-averaged velocity and boundary shear  
162 distribution of the same channels under different flow conditions. Figure 1(a) shows the plan  
163 view of experimental setup. Figure 1(b) shows the plan view of different test reach with cross-  
164 sectional dimensions of both NITR & Rezaei (2006) channels. Figure 1(c) shows the typical grid  
165 showing the arrangement of velocity measurement points along horizontal and vertical direction  
166 in the test section.

167  
168 A movable bridge was provided across the flume for both span-wise and stream-wise movements  
169 over the channel area so that each location on the plan of compound channel could be accessed  
170 for taking measurements. Water surface depths were measured directly with a point gauge  
171 located on an instrument carriage. The flow depth measurements were taken along the center of  
172 the flume at an interval of 0.5 m both in upstream and downstream prismatic parts of flume and  
173 at every 0.1 m in the converging part of the flume. A micro-Pitot tube of 4.77 mm external  
174 diameter in conjunction with suitable inclined manometer and a 16-Mhz Micro ADV (Acoustic  
175 Doppler Velocity-meter) was used to measure velocity at these points of the flow-grid. In some  
176 points, micro-ADV cannot take the velocity reading (up to 50cm from the water surface). In such  
177 points Pitot tube was used to take the velocity. The Pitot tube was physically rotated with respect  
178 to the main stream direction until it gave maximum deflection of the manometer reading. A flow  
179 direction finder having a minimum count of  $0.1^\circ$  was used to get the direction of maximum  
180 velocity with respect to the longitudinal flow direction. The angle of limb of Pitot tube with  
181 longitudinal direction of the channel was noted by the circular scale and pointer arrangement

182 attached to the flow direction meter. The overall discharge obtained from integrating the  
183 longitudinal velocity plot and from volumetric tank collection was found to be within  $\pm 3\%$  of the  
184 observed values. Using the velocity data, the boundary shear at various points on the channel  
185 beds and walls were evaluated from a semi log plot of velocity distribution.

186  
187  
188

### 3 NUMERICAL MODELING

189 A number of CFD packages (Fluent, CFX, Star-CD, and others) are now available and have been  
190 used for research in water flows Van Hoffa et al. (2010). In recent past, a good number of  
191 researchers have used these software packages for prediction of different aspects of 3D flow  
192 fields e.g Sahu et al. (2011). They detected that flow features in compound channels are  
193 dependent on topography of the channel, surface roughness etc. However, the flow behavior  
194 changes are still an unresolved phenomenon and attempts are underway to address this problem.  
195 These researchers attempted to predict the flow behavior using different numerical models as it is  
196 difficult to capture all flow features experimentally but still a lot of work is to be done. This is  
197 due to various problems which are encountered in numerical modelling such as grid generation,  
198 choice of turbulence model, discretization scheme, specifying the boundary and initial conditions  
199 etc.

200 In this work, an attempt has been made to improve the understanding of 3D flows in converging  
201 compound channels. For this purpose, a 3D numerical code FLUENT has been tested for its  
202 suitability for simulation of flood flows. Initially, the closure problem of governing equations  
203 was considered as there is no universal closure model which is acceptable for all flow problems.  
204 Each has its own advantages and disadvantages. Therefore, some consideration must be taken  
205 when choosing a turbulence model including, physics encompassed in the flow, level of accuracy  
206 and computation resources available one has to attempt different models and then to choose the  
207 one producing best results. The models tested here were standard  $k-\epsilon$ , LES and  $k-\omega$ . The one  
208 with best output (standard  $k-\omega$  in this case) was then used for all simulation works. The  $k-\omega$   
209 model is chosen on the basis of the computational time and resource availability. Beside the fact  
210 that  $k-\epsilon$  more or less produce same results as that of the  $k-\omega$  model but the other two-equation  
211 model 'k- $\omega$ ' performs better near the wall region and  $k-\epsilon$  performs better in the fully turbulent  
212 region (Filonovich 2015). On the other hand, LES partially resolves the turbulence and give good  
213 results when compared to experimental data (Kara et al. 2012). The overall idea of modelling  
214 through sub grid model for small time and length scale (Kolmogorov scales i.e. ratio of small  
215 eddies to large eddies lengthwise as well as time wise) and resolving the large scale through  
216 governing equation needs an exceptionally high computation effort. To optimize such  
217 computational resource and time requirement,  $k-\omega$  model is chosen even though compromises  
218 are made over the results which are acceptable than spending high in computational resources  
219 and time. It was used for prediction of resultant velocity contours on free surface, pressure,  
220 turbulence intensity and secondary flow velocities at different sections along the converging  
221 length.

222 Generally FLUENT involves three stage. The first stage is the pre-processing, which involve  
223 geometry creation, setting of grid and defining the physics of the problem. The second stage  
224 involves the application of solver to generate a numerical solution. In the third stage post-  
225 processing takes place, where the results are visualized and analyzed.

### 226 **3.1 Geometry**

227 The first step in CFD analysis is the explanation and creation of computational geometry of the  
228 fluid flow region. A consistent frame of reference for coordinate axis was adopted for creation of  
229 geometry. Here in coordinate system, x axis corresponded the lateral direction which indicates  
230 the width of channel bed. Y axis aligned stream-wise direction of fluid flow and Z axis  
231 represented the vertical component or aligned with depth of water in the channel. The origin was  
232 placed at the upstream boundary and coincided with the base of the center line of the channel.  
233 The water flowed along the positive direction of the y-axis. The simulation was done on a non-  
234 prismatic compound channel with a converging flood plain. The setup of the compound channel  
235 is shown in Figure 2.

236 For identify the domain six different surfaces are generated. Figure 3 shows the different  
237 Geometrical entities used in a non-prismatic compound channel

- 238 • Inlet
- 239 • Outlet
- 240 • Free Surface
- 241 • Side Wall
- 242 • Channel Bottom
- 243 • Centre line

244

### 245 **3.2 Mesh generation**

246

247 The second and very important step in numerical analysis is setting up the discretized grid  
248 associated with the geometry. Construction of the mesh involves discretizing or subdividing the  
249 geometry into the cells or elements at which the variables will be computed numerically. By  
250 using the Cartesian co-ordinate system, the fluid flow governing equations i.e. momentum  
251 equation, continuity equation are solved based on the discretization of domain. The meshing  
252 divides the continuum into a finite number of nodes. Generally, one of three different methods,  
253 i.e. Finite Element, Finite Volume and Finite Difference, can discretize the equations. Fluent  
254 uses Finite Element (FE) based Finite Volume Method (FVM). This alternative uses the control  
255 volume analysis, which is vertex-centered, i.e. the solution correlation variables are saved at the  
256 nodes (vertices) of the mesh. The concept of FVM is used to convert the partial differential  
257 equation into system of algebraic equation, which can be solved through closure. Two prominent  
258 discretization steps involved at this stage are discretization of the computational domain and  
259 discretization of the equation. The discretization of the computational domain is done through  
260 mesh generation, which can be identified later through control volume constructions. However, a  
261 very dense mesh of nodes causes excess computational time and memory. For CFD analysis,  
262 more nodes are required in some areas of interest, such as near wall and wake regions, in order to  
263 capture the large variation of fluid properties. Thus, the structure of grid lines causes further  
264 unnecessary use of computer storage due to further refinement of mesh. In this study, the flow  
265 domain is discretized using an unstructured grid and body-fitted coordinates. Unstructured grid is  
266 used so that intricacies can be covered under the grid which is left over in structured one. The  
267 detailed meshing of the flow domain is shown in Figure 4.

268

### 269 **3.3 Solver setting**

270

#### 271 *3.3.1 Setup*

272 After the meshing part is completed, various inputs are given in the Setup section. **VOF** (volume  
273 of fluid) model is the only model available for open channel flow simulation in ANSYS-  
274 FLUENT, which is based on the idea of volume fraction (Hirt and Nichols 1981). In this method,  
275 a transport equation is solved for the volume fraction at each time step whereupon the shape of  
276 the free surface is reconstructed explicitly using the distribution of the volume fraction function.  
277 The “reconstruction” of the free surface can be explained more clearly through the concept of  
278 water volume fraction. Free surface is defined as the cell, which takes the value of the water  
279 volume fraction as non-zero while a zero value indicates that no fluid is present in the cell. The  
280 value of 0.5 for the water volume fraction is indicative of the fact that free surface position is  
281 detected. This method can define sharp interfaces and is robust. VOF is capable of calculating  
282 time dependent solutions. Flow in an open channel is generally bound by channel from all  
283 directions except for the upward free surface. To achieve a free surface zero friction interface, a  
284 command called “surface\_symmetry” is given in named selection. Velocity inlet for inlet and  
285 pressure outlet for outlet is defined and the roughness coefficient is added to the walls for “no  
286 slip” condition. Transient flow was chosen because the flow parameters were varied in time in  
287 the experiment. Gravity is check marked and the value for Z-axis is given as -9.81 because  
288 gravity acts downward opposite to the z-direction vector. As mentioned earlier, the turbulence  
289 model was chosen as k-  $\omega$  model. PISO was selected for solving the pressure equation, as it is  
290 generally a pressure-based segregated algorithm recommended for transient flow conditions (Issa  
291 1986). Also, PISO scheme may aid in accelerating convergence for many unsteady flows.  
292 Finally, solver is patched and run to apply all the settings as well as conditions mentioned above.  
293 It’s just finalizing and complying the settings. The equation solved in the CFD are usually  
294 iterative and starting from initial approximation, they iterate to a final result. However, these  
295 iterations are terminated at some step to minimize the numerical effort. This termination are done  
296 on the basis of normalized residual target which is by default is set to  $10^{-4}$ , which leads to loose  
297 convergence target. For problems like compound channel in order to obtain more accuracy  
298 residual target should be placed a value near around  $10^{-6}$ . Time step size was set to 0.001s and  
299 number of iteration given was 1000 for better accuracy and convergence of the iteration. Time  
300 step size,  $\Delta t$ , is then set in the Iterate panel,  $\Delta t$  must be small enough to resolve time-dependent  
301 features; making sure that the convergence is reached within the number of max iterations per  
302 time step. The order of magnitude of an appropriate time step size can be estimated as ratio of  
303 typical cell size to the characteristic flow velocity. Time step size estimate can also be chosen so  
304 that the unsteady characteristics of the flow can be resolved (e.g. flow within a known period of  
305 fluctuations). To iterate without advancing in time, use zero time steps.

306

### 307 *3.3.2 Governing Equations*

308 ANSYS Fluent uses the finite volume method to solve the governing equations for a fluid. It  
309 provides the capability to use different physical models such as incompressible or compressible,  
310 inviscid or viscous, laminar or turbulent etc. The most practical and still the most popular  
311 method of dealing with turbulence is that based on the RANS method. With this method, all  
312 scales of turbulence are modelled. Several models were studied to compare the effect of  
313 turbulent modeling in the converging compound channel, including the following: (1) k-Epsilon,  
314 (2)  $k-\omega$  and (3) Large Eddy Simulation (LES) model. Here  $k-\omega$  model is used for turbulence  
315 modeling. The  $k-\omega$  model solves the  $k$ -transport equation and a transport equation for  $\omega$ . The  $k$ -  
316 transport equation and the transport equation for  $\omega$  can be written (Wilcox 1988)

317

318 
$$\frac{\partial k}{\partial t} + U_i \frac{\partial k}{\partial x_i} = \frac{\partial}{\partial x_i} \left( \frac{v_t}{\sigma_k} \frac{\partial k}{\partial x_i} \right) + P - \beta' k \omega \quad (1)$$

319  
320 
$$\frac{\partial \omega}{\partial t} + U_i \frac{\partial \omega}{\partial x_i} = \frac{\partial}{\partial x_i} \left( \frac{v_t}{\sigma_\omega} \frac{\partial \omega}{\partial x_i} \right) + \alpha \frac{\omega}{k} P - \beta \omega^2 \quad (2)$$

321  
322 and the eddy viscosity is given by

323  
324 
$$v_t = k / \omega \quad (3)$$

325  
326  $P$  is the turbulence kinetic energy production rate. Menter [49] as suggested the turbulence  
327 equation:

328  
329 
$$P = \min (P, 10\beta' k \omega) \quad (4)$$

330 It represents the rate at which the energy is fed from the mean flow to each stress component.  
331 The estimation of the production term can be done directly from the stress and the mean flow  
332 strain rate components and thus needs no modelling other than this all other terms need  
333 modelling.

334 The  $k-\omega$  model involves five empirical constants  $\beta'$ ,  $\beta$ ,  $\alpha$ ,  $\sigma_k$  and  $\sigma_\omega$ . They have their universal  
335 constant values, which have been derived on the basis of high quality data. Their values vary  
336 from one turbulence model to another. For any particular turbulence model, the values of these  
337 constants remain same for all simulation purposes. For standard  $k-\omega$ , their values are presented in  
338 Table 2.

339  
340 *3.3.3 Boundary conditions*

341 Four different types of boundary condition were considered in this study. These are (i) inlet, (ii)  
342 outlet, (iii) water surface, and (iv) walls of the geometry

343 *(i) Inlet*

344 The velocity distribution at the upstream cross-section was taken as inlet boundary condition. At  
345 the inlet, turbulence properties i.e.  $k$  (turbulence kinetic energy) and ( $\omega$  turbulence dissipation  
346 rate) must be specified. These were calculated as [28]

347  
348 
$$k = IU^2 \quad (5)$$

349  
350 
$$\omega = \frac{k^{1/2}}{l} \quad (6)$$

351  
352 Where  $I$  is the turbulence intensity and  $U$  is the mean value of stream-wise velocity.  $l$  is the  
353 turbulence length scale

354 *(ii) Outlet*

355 At the outlet, the pressure condition was given as the boundary condition and pressure was fixed  
356 at zero. Importance of the outflow boundary at an appropriate location can be explained through  
357 the influence of the downstream condition. Thus it makes extremely imperative to put the  
358 downstream end far enough to prevail the fully developed state.

359 *(iii) Channel and Floodplain Boundaries*

360 A no-slip boundary condition was considered at the walls. This means that the velocity  
361 components should be zero at the walls. The no-slip condition is the default, and it indicates that

362 the fluid sticks to the wall and moves with the same velocity as the wall, if it is moving. The wall  
363 is the most common boundary condition in bounded fluid flow problem. Setting the velocity near  
364 wall as zero under no-slip condition is appropriate condition for the solid boundary. The wall  
365 boundary condition in the turbulent flow is implemented and initiated by evaluating the  
366 dimensionless distance ' $z^+$ ' from the wall to the nearest boundary node. This dimensionless  
367 distance is the function of the near wall node to the solid boundary, friction velocity and the  
368 kinematic viscosity. The near wall treatment will depend on the position of the nearest to the  
369 boundary node. If  $z^+ \leq 11.06$  the nearest to boundary node will lie in the viscous sub-laminar  
370 layer where profile is linear and very fine meshing is required. This will tend to intensify the  
371 computation effort, which is being dedicated for near wall treatment. In another case where  
372  $z^+ > 11.06$  the nearest boundary node will lie in the buffer layer which is the transition region  
373 from viscous sublayer and the log law region. The main shortcoming of the wall function  
374 approach is their dependability on the nearest node distance from the wall, which cannot be  
375 overcome through refining since it does not guarantees high accuracy. Nevertheless, the problem  
376 of discrepancy in the wall function approach can be subsidized through Scalable wall function  
377 where limiting the  $z^+$  value to not fall below 11.06 (the intersection of linear profile and log-law)  
378 is concentrated. Therefore, all mesh points are made lie outside the viscous sublayer and all fine  
379 mesh discrepancies are circumvented.

380 Thus, standard wall-function, which uses log-law of the wall to compute the wall shear stress is,  
381 used [50]. Fluid flows over rough surfaces are encountered in diverse situations. If the modeling  
382 is a turbulent wall-bounded flow in which the wall roughness effects are considered significant,  
383 it can include the wall roughness effects through the law-of-the-wall modified for roughness.

#### 384 (iv) Free Surface

385 The water surface was defined as a plane of symmetry, which means that the normal velocity and  
386 normal gradients of all variables are zero at this plane. Free surface in the present study is  
387 modeled through VOF for estimating the domain for air and water (multiphase problem).  
388

### 389 3.4 Results

390 A variety of flow characteristics can be considered in the post-processing software of CFD  
391 packages. This work has been concerned with the velocity distribution and the results are  
392 compared with experimental measurements. In general the user should make an attempt to  
393 validate the CFD results with known data so that there can be some confidence in the solution. In  
394 the case of open channel flow, the validation is most likely to take the form of a comparison  
395 against physical measurements and a qualitative understanding of what features should be  
396 present in the flow. As part of the analysis, the user may also wish to perform a sensitivity study  
397 and vary any parameters (such as roughness here) which have a degree of uncertainty, and  
398 determine what influence they have on the solution.  
399

## 400 4. PREDICTION USING ANN

401  
402 ANN is a new and rapidly growing computational technique and an alternative procedure to  
403 tackle complex problems. In recent years it has been broadly used in hydraulic engineering and

404 water resources [36, 37]. It is a highly self-organized, self-adapted and self-trainable  
 405 approximator with high associative memory and nonlinear mapping. ANNs may consist of  
 406 multiple layers of nodes interconnected with other nodes in the same or different layers. Various  
 407 layers are referred to as the input layer, the hidden layer and the output layer. The inputs and the  
 408 inter-connected weights are processed by a weight summation function to produce a sum that is  
 409 passed to a transfer function. The output of the transfer function is the output of the node. In this  
 410 paper, multi-layer perception network is used. Input layer receives information from the external  
 411 source and passes this information to the network for processing. Hidden layer receives  
 412 information from the input layer and does all the information processing, and output layer  
 413 receives processed information from the network and sends the results out to an external  
 414 receptor. The input signals are modified by interconnection weight, known as weight factor  $W_{ij}$   
 415 which represents the interconnection of  $i^{th}$  node of the first layer to the  $j^{th}$  node of the second  
 416 layer. The sum of modified signals (total activation) is then modified by a sigmoidal transfer  
 417 function ( $f$ ). Similarly output signals of hidden layer are modified by interconnection weight  
 418 ( $W_{ij}$ ) of  $k^{th}$  node of output layer to the  $j^{th}$  node of the hidden layer. The sum modified  $k$  signal is  
 419 then modified by a pure linear transfer function ( $f$ ) and output is collected at output layer.

420  
 421 Let  $I_p = (I_{p1}, I_{p2}, \dots, I_{pl})$ ,  $p=1, 2, \dots, N$  be the  $p^{th}$  pattern among  $N$  input patterns.  $W_{ji}$  and  $W_{kj}$  are  
 422 connection weights between  $i^{th}$  input neuron to  $j^{th}$  hidden neuron and  $j^{th}$  hidden neuron to  $k^{th}$   
 423 output neuron respectively.

424 Output from a neuron in the input layer is

$$425 \quad O_{pi} = I_{pi}, i=1, 2 \dots l \quad (7)$$

426  
 427 Output from a neuron in the hidden layer is

$$428 \quad O_{pj} = f(NET_{pj}) = f(\sum_{i=0}^l W_{ji} O_{pi}), j = 1, 2, m \quad (8)$$

429  
 430 Output from a neuron in the hidden layer is

$$431 \quad O_{pk} = f(NET_{pk}) = f(\sum_{i=0}^l W_{kj} O_{pj}), k=1, 2, n \quad (9)$$

432  
 433

#### 436 **4.1 Sigmoidal Function**

437 A bounded, monotonic, non-decreasing, S Shaped function provides a graded non-linear  
 438 response. It includes the logistic sigmoid function

$$439 \quad F(x) = \frac{1}{1+e^{-x}} \quad (10)$$

440 Where  $x$  = input parameters taken

441  
 442 The architecture of back propagation neural network model, that is the  $l$ - $m$ - $n$  ( $l$  input neurons,  $m$   
 443 hidden neurons, and  $n$  output neurons) is shown in the fig.5

#### 444 445 **4.2 Learning or training in back propagation neural network**

446 Batch mode type of supervised learning has been used in the present case in which  
447 interconnection weights are adjusted using delta rule algorithm after sending the entire training  
448 sample to the network. During training, the predicted output is compared with the desired output  
449 and the mean square error is calculated. If the mean square error is more, then a prescribed  
450 limiting value, it is back propagated from output to input and weights are further modified until  
451 the error or number of iteration is within a prescribed limit.

452 Mean Squared Error,  $E_p$  for pattern is defined as

$$453 \quad E_p = \sum_{i=1}^n \frac{1}{2} (D_{pi} - O_{pi})^2 \quad (11)$$

454 Where  $D_{pi}$  is the target output,  $O_{pi}$  is the computed output for the  $i^{th}$  pattern.

455 Weight changes at any time  $t$ , is given by

$$456 \quad \Delta W(t) = -nE_p(t) + \alpha \times \Delta W(t - 1) \quad (12)$$

457  $n$  = learning rate i.e.  $0 < n < 1$

458  $\alpha$  = momentum coefficient i.e.  $0 < \alpha < 1$

### 459 **4.3 Source of data**

460 The data are collected from research work done in Hydraulic and Fluid Mechanics Laboratory,  
461 NIT Rourkela, [44] data, available at the laboratory of University of Birmingham, Wallingford  
462 and also generated data by using ANSYS-15 .The descriptions of geometrical parameters of  
463 above data are mentioned in Table.3.

464

### 465 **4.4 Selection of hydraulic parameters**

466 Flow hydraulics and momentum exchange in converging compound channels are significantly  
467 influenced by both geometrical and hydraulic variables, the computation become more complex  
468 when the floodplain width contracted and become zero. The flow factors responsible for the  
469 estimation of depth-averaged velocities are

470 (i) Converging angle denoted as  $\theta$

471 (ii) Width ratio ( $\alpha$ ) i.e .ratio of width of floodplain to width of main channel

472 (iii) Aspect ratio ( $\sigma$ ) i.e. ratio of width of main channel (B) to depth of main channel (h)

473 (iv) Depth ratio ( $\beta$ ) =  $(H-h)/H$ , where  $H$ =height of water at a particular section and,  $h$ = height of  
474 water in main channel

475 (v) Relative distance ( $X_r$ ) i.e of point velocity in the length wise direction of the channel)/total  
476 length of the non-prismatic channel. Total five flow variables were chosen as input parameters  
477 and depth-averaged velocity as output parameter.

478

## 479 **5. RESULTS**

480

### 481 **5.1 Results of ANSYS and CES**

482

#### 483 *5.1.1 Verification*

484 The values of depth-averaged velocity distributions of different cross-sections of the non-  
485 prismatic compound channel are achieved from the numerical models like CES (Conveyance  
486 Estimating System) and ANSYS then the results from the experimental data of both NITR and  
487 [44] channels were compared in Figures 6-11. As illustrated in Figures 6-10, the numerical  
488 model was in good agreement with experimental results but the results of the CES model have  
489 some differences with experimental results. The Conveyance and Afflux Estimation System  
490 (CES/AES) is a software tool for the improved estimation of flood and drainage water levels in  
491 rivers, watercourses and drainage channels. The software development followed  
492 recommendations by practitioners and academics in the UK Network on Conveyance in River  
493 Flood Plain Systems, following the Autumn 2000 floods, that operating authorities should make  
494 better use of recent improved knowledge on conveyance and related flood (or drainage) level  
495 estimation. This led to a Targeted Program of Research aimed at improving conveyance  
496 estimation and integration with other research on afflux at bridges and structures at high flows.  
497 The CES/AES software tool aims to improve and assist with the estimation of:

- 498 • hydraulic roughness
- 499 • water levels (and corresponding channel and structure conveyance)
- 500 • flow (given slope)
- 501 • section-average and spatial velocities
- 502 • backwater profiles upstream of a known flow-head control e.g. weir (steady)
- 503 • afflux upstream of bridges and culverts
- 504 • uncertainty in accuracy of input data and output

505 Conveyance Estimation System (CES) is developed by joint Agency/DEFRA research program  
506 on flood defence, with contributions from the Scottish Executive and the Northern Ireland Rivers  
507 Agency, HR Wallingford. CES is based Reynolds-averaged Navier-Stokes (RANS) approach as  
508 the solution basis for estimation of conveyance. RANS equation of CES has been solved  
509 analytically by Shiono & Knight method. In this solution the converging fluid plain effect has  
510 not been considered which is reflected by the results of depth-averaged velocity and giving much  
511 error However, Fluent K- $\omega$  model take care of converging effect as well as interaction effect of  
512 geometry of converging compound channel.

513

## 514 **5.2 Results of ANN**

### 515 *5.2.1 Testing of Back propagation neural network*

516 Determination of depth-averaged velocity distribution of compound channel with converging  
517 flood plain is an important task for river engineer. Due to nonlinear relationship between the  
518 dependent and independent variables any model tools to provide the accurate depth-averaged  
519 velocity distribution. Numerical approach has also consumed more memory and time. So in the  
520 present work the ANN has been tested. The total experimental data set is divided into training set  
521 and testing set. For depth-averaged velocity calculations 32321 data are used among which 70%  
522 are training data and 30% are taken as testing data. The number of layers and neurons in the  
523 hidden layer are fixed through exhaustive experimentation when mean square error is minimised  
524 for training data set. It is observed that minimum error is obtained for 5-7-1 architecture. So the  
525 back propagation neural network (BPNN) used in this work has three layered feed forward  
526 architecture. The model was run on MATLAB commercial software dealing with trial and error  
527 procedure.

528

529 A regression curve is plotted between actual and predicted depth-averaged velocity of testing  
530 data which are shown in figure (12) .It can be observed that data are well fitted because a high

531 degree of coefficient of determination  $R^2$  of 0.91. Figure 13 shows the error histogram plot of the  
532 model.

533

## 534 **6. ERROR ANALYSIS**

535

536 To check the strength of the model, with the result from CES error analyses have been done.  
537 Mean Absolute Error (MAE), the Mean Absolute Percentage Error (MAPE), Mean Squared  
538 Error (MSE), the Root Mean Squared Error (RMSE) for all the converging compound channels  
539 for different geometry and flow conditions have been estimated. Efficiency criterion like  $R^2$ ,  
540 Nash-Sutcliffe efficiency (E) have also been estimated to provide more information on the  
541 systematic and dynamic errors present in the model simulation. The definitions of error terms are  
542 described below. The detailed results of the error analysis have been presented in table 4 .The  
543 expression used to estimate errors in different forms are

### 544 **1. Mean Absolute Error (MAE)**

545 The Mean Absolute Error has been evaluated as,

546

$$547 \quad MAE = \frac{1}{n} \sum_i^n \left| \frac{P_i - O_i}{O_i} \right| \quad (13)$$

548

549 Where  $P_i$ =predicted values,  $O_i$ =observed values

550

### 551 **2. Mean Absolute Percentage Error (MAPE)**

552 Mean Absolute Percentage Error also known as Mean absolute Percentage Deviation. It was  
553 usually expressed as a percentage, and was defined by the formula

554

$$555 \quad MAPE = \frac{1}{n} \sum_i^n \left| \frac{O_i - P_i}{O_i} \right| \quad (14)$$

### 556 **3. Mean Squared Error (MSE)**

557 Mean Squared Error measures the average of the squares of the errors. It is computed as

$$558 \quad MSE = \frac{1}{n} \sum_i^n (P_i - O_i)^2 \quad (15)$$

### 559 **4. Root Mean Squared Error (RMSE)**

560 Root Mean Squared Error or Root Mean Squared Deviation is also a measure of the differences  
561 between values predicted by model or an estimator and the actually observed values. These  
562 individual differences are called as residuals when the calculations are performed over the data  
563 sample that is used for estimation, and are known as estimation errors when computed out  
564 of the sample. The RMSE is defined as

565

$$566 \quad RMSE = \sqrt{MSE} \quad (16)$$

### 567 **5. Coefficient of correlation $R^2$**

568 The coefficient of correlation  $R^2$  can be expressed as the squared ratio between the covariance  
569 and the multiplied standard deviations of the observed and predicted values. The range of  $R^2$  lies  
570 between 0 and 1.0 which describes how much of the observed dispersion is explained by the  
571 prediction. A value of zero means no correlation at all whereas a value of 1 means that the  
572 dispersion of the prediction is equal to that of the observation.

573  
574

## 575 6. Nash-Sutcliffe efficiency E

576 The efficiency E proposed by Nash and Sutcliffe [51] is defined as:

$$577 E = 1 - \frac{\sum_i^n (O_i - P_i)^2}{\sum_i^n (O_i - \bar{O})^2} \quad (17)$$

578 Where  $\bar{O}$  represents the mean of calculated values. The range of E lies between 1.0 (perfect fit)  
579 and  $-\infty$ .

580

## 581 7. CONCLUSIONS

582

583 In this study numerical analysis for prediction of depth-averaged velocity for compound channel  
584 with converging flood plain using ANN were presented. In the first part of the paper, a 3D model  
585 of turbulence stream pattern in compound channel with converging flood plains were simulated  
586 using a numerical model. Using experimental and numerical analysis, variation of velocity  
587 components for compound channel with converging flood plains were studied. The other part of  
588 this paper dealt with the prediction of the depth-averaged velocity field using ANN. In the  
589 prediction part, at first, BPNN neural networks were created. Then coordinates of different points  
590 were applied as input values and corresponding velocity as target outputs to create ANNs. Some  
591 experimental data were used to train the ANNs and some experimental data were used to test the  
592 trained ANNs based on BPNN techniques. Finally, the results of ANN and CES methods were  
593 compared in sections. The main conclusions of this study are as follows:

594

595 1. ANSYS shows a good conformity with the experimental results for predicting the depth-  
596 averaged velocity.

597

598 2. Results of numerical model showed that the CES was not in good agreement with  
599 experimental results for predicting the depth-averaged velocity. Since the one dimensional model  
600 of CES is incompetent when it comes to more realistic results.

601

602 3. Results of ANNs that had been trained using BPNN indicated that the velocity field was  
603 predicted with good approximation in both training and testing methods and it was concluded  
604 that the proposed procedures are useful for velocity prediction in non-prismatic compound  
605 channel with converging flood plain.

606

607 4. Different error analyses are performed to test the strength of the present ANN model. It is  
608 found that MAE as 0.033, MAPE as 3.29 which less than 10%, MSE as 0.0004, RMSE as 0.02, E

609 as 0.0.95,  $R^2$  as 0.99 where as CES gave MAE as 0.2, MAPE as 20, MSE as 0.008, RMSE as  
610 0.08, E as 0.75,  $R^2$  as 0.7.

611  
612 5. The main advantage of ANN is the prediction of the approximate velocity at points where  
613 experimental data are not available. In addition, the presented procedure can be used in  
614 predicting some other properties of flow besides velocity, such as shear stresses, depth of water  
615 or variations of channel bed. In addition, the presented procedure can be applied to prediction  
616 and analysis of the properties of other types of channels and other structures across the flow.

617  
618 Turbulence studies can also be carried out on the same guidelines indicating the turbulent  
619 shearing through Reynolds stresses, secondary flow structures, and the turbulent kinetic energy,  
620 which can significantly indicate the momentum exchange process and mass transfer due to  
621 differential velocity due to two different stages. Overall studies consider only depth averaged  
622 streamwise velocity prediction only, since the applicability of numerical modelling is  
623 corroborated on the converging compound channel. Since the validation and error analysis shows  
624 an undisputable results, which suggestively indicate the application of the numerical method for  
625 further studies such as turbulence studies.

## 626 627 **8. ACKNOWLEDGEMENTS**

628  
629 The author wish to acknowledge the support from the Institute and the UGC UKIERI Research  
630 project (ref no UGC-2013 14/017) by the second authors for carrying out the research work in  
631 the Hydraulics Laboratory at National Institute of Technology, Rourkela.

## 632 633 634 635 **9. REFERENCES**

- 636  
637 1. Abdeen, M. A. M. (2008). Predicting the impact of vegetations in open channels with  
638 different distributaries' operations on water surface profile using artificial neural  
639 networks. *Journal of Mechanical Science and Technology*, 22, 1830–1842.
- 640 2. Bhattacharya, B. & Solomatine, D. P. (2005). Neural networks and M5 model trees in  
641 modelling water level–discharge relationship. *Neurocomputing*, 63, 381–396.
- 642 3. Bilgil, A., Altun, H. (2008). Investigation of flow resistance in smooth open channels  
643 using artificial neural networks. *Flow Measurement and Instrumentation* 19, 404-408.
- 644 4. Cater, J. E. and Williams, J. J. R. (2008). Large eddy simulation of a long asymmetric  
645 compound open channel.
- 646 5. Cheng, C.T., Ou, C.P., Chau, K.W. (2002). Combining a fuzzy optimal model with  
647 a genetic algorithm to solve multi-objective rainfall–runoff model calibration. *Journal of*  
648 *Hydrology* 268, 72–86.
- 649 6. Cokljat, D. (1993). Turbulence Models for Non-circular Ducts and Channels. PhD  
650 Thesis, City University London.
- 651 7. Ervine, D. A., Koopaei K. B. and Sellin R. H. J. (2000). Two Dimensional Solution for  
652 Straight and Meandering Over-bank Flows. *J. Hydraul. Eng., ASCE*, 126 (9), 653-669.

- 653 8. Filonovich MS, Azevedo R, Rojas-Solórzano L, Leal, JB (2013). Credibility Analysis of  
654 Computational Fluid Dynamic Simulations for Compound Channel Flow. *Journal of*  
655 *Hydroinformatics* 15(3), 926-938.
- 656 9. Gandhi, B.K., Verma, H.K., Abraham, B.(2010). Investigation of Flow Profile in Open  
657 Channels using CFD, 8th Intl Conference on Hydraulic Efficiency Measurement, 243-  
658 251.
- 659 10. Ghosh, S., and Jena, S.B. (1971). Boundary shear stress distribution in open channel  
660 compound. *Proc. Inst. Civil Eng.* 49, 417–430.
- 661 11. Ghosh, S., Pratihari, D.K., Maiti, B., Das, P.K. (2010). Optimum design of a two step  
662 planar diffuser: A hybrid approach. *Engineering Applications of Computational Fluid*  
663 *Mechanics* 4(3), 415-424.
- 664 12. Hodges, B. R., & Street, R. L. (1999). On simulation of turbulent nonlinear free-surface  
665 flows. *J. Comp. Phys.* 151, 425–457.
- 666 13. Hodkinson, A., and R. Ferguson,(1998). Numerical modelling of separated flow in river  
667 bends: model testing and experimental investigation of geometric controls on the extent  
668 of flow separation at the concave bank. *Hydrological Processes*, 12, 1323-1338.
- 669 14. Hodkinson, A.,(1996). Computational fluid dynamics as a tool for investigating  
670 separated flow in river bends. *Earth Surface Processes and Landforms*,21, 993-1000.
- 671 15. Hsu, T. Y., Grega, L. M., Leighton, R. I. and Wei, T. (2000). Turbulent kinetic energy  
672 transport in a corner formed by a solid wall and a free surface. *J. Fluid Mech.* 410, 343-  
673 366.
- 674 16. Issa, R. I. (1986). Solution of the implicitly discretised fluid flow equations by operator-  
675 splitting. *Journal of computational physics*, 62(1), 40-65.
- 676 17. *J. Hydraulic Research* 46 (4), 445-453.
- 677 18. Jain, S. K. (2008).Development of integrated discharge and sediment rating relation using  
678 a compound neural network. *Journal of Hydrologic Engineering* 13, 124–131.
- 679 19. Kara, S., Stoesser, T. and Sturm, T. W. (2012). Turbulence statistics in compound  
680 channels with deep and shallow overbank flows. *J. Hydraulic Research* 50 (5), 482-493.
- 681 20. Kawahara, Y., & Tamai, N. (1988). Numerical calculation of turbulent flows in  
682 compound channels with an algebraic stress turbulence model. In: *Proc. 3rd Symp.*  
683 *Refined Flow Modeling and Turbulence Measurements*, Tokyo, Japan, pp. 9–17.
- 684 21. Khatua K.K, Patra K C, Mohanty, P.K. (2012). Stage Discharge Prediction for Straight  
685 and Smooth Compound Channels with Wide Floodplains. *J. Hydraul. Eng., ASCE*, 138  
686 (1), 93-99.
- 687 22. Khatua, K.K., Patra, K.C. (2008). Boundary Shear Stress Distribution in Compound  
688 Open Channel Flow. *J. Hydraul. Eng., ISH*, 12 (3), 39-55.
- 689 23. Knight, D. W., Wright, N. G. and Morvan, H. P. (2005) .Guidelines for applying  
690 commercial CFD software
- 691 24. Krishnappan, B. G., and Lau, Y. L. 1986. Turbulence modelling of flood plain flows. *J.*  
692 *Hydraulic Eng., ASCE*, 112(4), 251-266.
- 693 25. Lane S. N., Bradbrook, K. F., Richards, K. S., Biron, P. A. & Roy, A. G. (1999). The  
694 application of computational fluid dynamics to natural river channels: three-dimensional  
695 versus two dimensional approaches. *Geomorphology* 29, 1–20.
- 696 26. Lin, J.Y., Cheng, C.T., Chau, K.W. (2006). Using support vector machines for long-term  
697 discharge prediction. *Hydrological Sciences Journal* 51(4): 599-612.

- 698 27. Menter, F. R. (1994) .Two-equation eddy-viscosity turbulence models for engineering  
699 applications. *AIAA*, 32 (8), 1598 – 1605.
- 700 28. Morvan, H. P.(2001). Three-dimensional Simulation of River Flood Flows. PhD  
701 Thesis,University of Glasgow, Glasgow.
- 702 29. Muzzammil, M. (2008). Application of neural networks to scour depth prediction at the  
703 bridge abutments. *Engineering Applications of Computational Fluid Mechanics* 2(1), 30-  
704 40.
- 705 30. Myers,W. R. C., and Elsayy (1975). Boundary Shear in Channel with Floodplain. *J.*  
706 *Hydraul. Eng.*, ASCE, 101(HY7), 933-946.
- 707 31. Nakayama, A. & Yokojima, S. (2002). LES of open-channel flow with free-surface  
708 fluctuations. In: *Proc. Hydraul. Eng. JSCE*. 46, 373–378.
- 709 32. NASH, J. E., SUTCLIFFE, J. V.(1970). River flow forecasting through conceptual  
710 models, Part I. A discussion of principles.*J. Hydrol.* 10, 282–290.
- 711 33. Pan, Y., & Banerjee, S. (1995). Numerical investigation of free-surface turbulence in  
712 open-channel flows. *Phys. Fluids* ,113 (7),1649–1664.
- 713 34. Rezaei, B.(2006). Overbank flow in compound channels with prismatic and non-  
714 prismatic floodplains. PhD Thesis. Univ. of Birmingham. U.K.
- 715 35. Rhodes, D. G., and Knight, D. W. (1994). Distribution of Shear Force on Boundary of  
716 Smooth Rectangular Duct. *Journal of Hydraulic Engg.*, 120-7, 787– 807.
- 717 36. Safikhani, H., Khalkhali, A., Farajpoor, M. (2011). Pareto Based Multi-Objective  
718 Optimization of Centrifugal Pumps Using CFD, Neural Networks and Genetic  
719 Algorithms. *Engineering Applications of Computational Fluid Mechanics* 5(1), 37-48.
- 720 37. Sahu, M., Khatua, K. K. & Mahapatra, S. S. (2011). A neural network approach for  
721 prediction of discharge in straight compound open channel flow. *Flow Measurement and*  
722 *Instrumentation*, 22, 438–446.
- 723 38. Shiono, K., Knight, D. W. (1988). Refined Modelling and Turbulence Measurements.  
724 *Proceedings of 3rd International Symposium, IAHR, Tokyo, Japan, July, 26-28.*
- 725 39. Sinha, S. K., Sotiropoulos, F. & Odgaard, A. J.(1998). Three dimensional numerical  
726 model for flow through natural rivers.*J. Hydraul. Eng.* 124(1), 13–24.
- 727 40. Spalding, D. B. (1980) .*Genmix: a general computer program for two-dimensional*  
728 *parabolic phenomena*, Pergamon Press, Oxford.
- 729 41. Speziale, C. G., Sarkar, S. and Gatski, T. B. (1991) .Modelling the pressure-strain  
730 correlation of turbulence: an invariant dynamical systems approach. *J. Fluid Mech.* 277,  
731 245-272.
- 732 42. Thomas, T. G. and Williams, J. J. R. (1995a). Large eddy simulation of turbulent flow in  
733 an asymmetric compound channel. *J. Hydraulic Research* 33 (1), 27-41.
- 734 43. to open channel flow. Report based on the research work conducted under EPSRC Grants  
735 GR/R43716/01 and GR/R43723/01.
- 736 44. Unal, B., Mamak, M., Seckin, G. & Cobaner, M. (2010). Comparison of an ANN  
737 approach with 1-D and 2-D methods for estimating discharge capacity of straight  
738 compound channels. *Advances in Engineering Software*, 41, 120–129.
- 739 45. Van Hooff, T., & Blocken, B. (2010). Coupled urban wind flow and indoor natural  
740 ventilation modelling on a high-resolution grid: A case study for the Amsterdam Arena  
741 stadium. *Environmental Modelling & Software*, 25(1), 51-65.

- 742 46. Van Hooff, T., and Bert Blocken. "Coupled urban wind flow and indoor natural  
743 ventilation modelling on a high-resolution grid: A case study for the Amsterdam Arena  
744 stadium." *Environmental Modelling & Software* 25.1 (2010): 51-65.
- 745 47. Wang, W.C., Chau, K.W., Cheng, C.T., Qiu, L. (2009). A comparison of performance of  
746 several artificial intelligence methods for forecasting monthly discharge time series.  
747 *Journal of Hydrology* 374, 294-306.
- 748 48. Wilcox, D. C. 1988. Reassessment of the scale-determining equation for advanced  
749 turbulence models. *AIAA*, 26, 1299–1310.
- 750 49. Wu, C.L., Chau, K.W., Li, Y.S. (2009). Predicting monthly streamflow using data-driven  
751 models coupled with data-preprocessing techniques. *Water Resources Research* 45, 1-23.
- 752 50. Xie, Z., Lin, B. and Falconer, R. A. (2013). Large-eddy simulation of the turbulent  
753 structure in compound open-channel flows. *Advances in Water Resources* 53, 66-75.
- 754 51. Yuhong, Z., Wenxin, H. (2009). Application of artificial neural network to predict the  
755 friction factor of open channel flow. *Communications in Nonlinear Science and*  
756 *Numerical Simulation* 14, 2373-2378.
- 757

**Table1.**Hydraulic parameters for the experimental channel data

Sl. No	Item Description	Converging Compound Channel
1	Geometry of main channel	Rectangular
2	Geometry of flood plain	Converging
3	Main channel width (b)	0.5m
4	Bank full depth of main channel	0.1m
5	Top width of compound channel (B1)	before convergence 0.9m
6	Top width of compound channel (B2)	after convergence 0.5m
7	Converging length of the channels	0.84m, 1.26, 2.26m
8	Slope of the channel	0.0011
9	Angle of convergence of flood plain ( $\theta$ )	12.38,9, 5
10	Position of experimental section 1	start of the converging part
11	Position of experimental section 2	Middle of converging part
12	Position of experimental section	end of converging part.

**Table 2.** Values of the constants in the k-  $\omega$  model (Wilcox 1988)

$\beta'$	$\beta$	$\alpha$	$\sigma_k$	$\sigma_\omega$
0.09	0.075	5/9	2	2

**Table 3.**Input and output data used for the present analysis

Sl.No	Converging angles	Flood plain type	Converging Length
1	1.91	Convergent	6m
2	3.81	Convergent	6m
3	11.31	Convergent	2m
4	5	Convergent	2.26m
5	9	Convergent	1.28m
6	12.38	Convergent	0.84m
8	2.5	Convergent	4.58
9	3	Convergent	3.82
10	4	Convergent	2.86
11	7	Convergent	1.64
12	10	Convergent	1.15
13	14	Convergent	0.8
14	15	Convergent	0.77

---

15	17	Convergent	0.68
16	20	Convergent	0.58

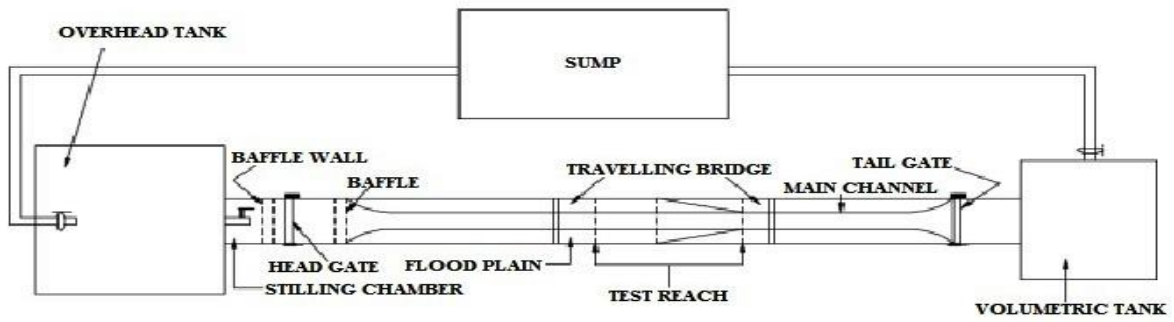
---

Table 4 Different Error Analysis

---

	ANN	CES
MSE	0.0004	0.008
RMSE	0.02	0.08
MAE	0.033	0.2
MAPE	3.29	20
E	0.95	0.70
R <sup>2</sup>	0.99	0.75

---



**Figure 1(a).** Plan view of Experimental Setup

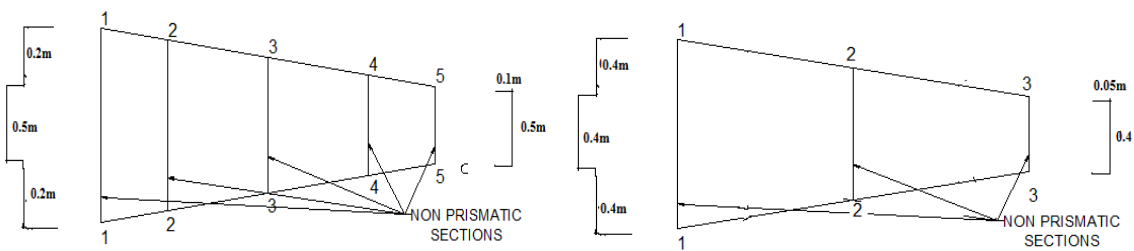


**Figure 1(b).** Plan view of different test reaches with cross-sectional dimensions of non-prismatic compound channel from both NITR & Rezaei (2006) channels

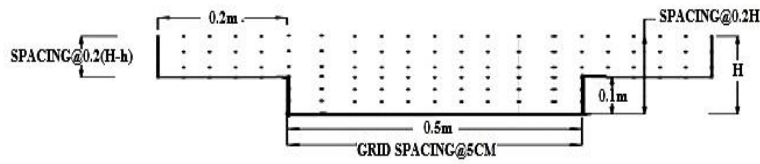
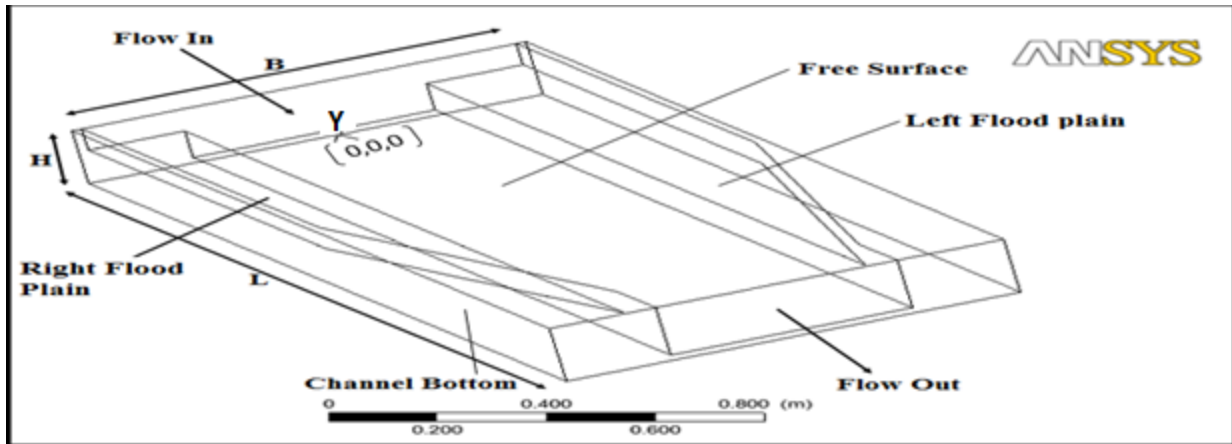
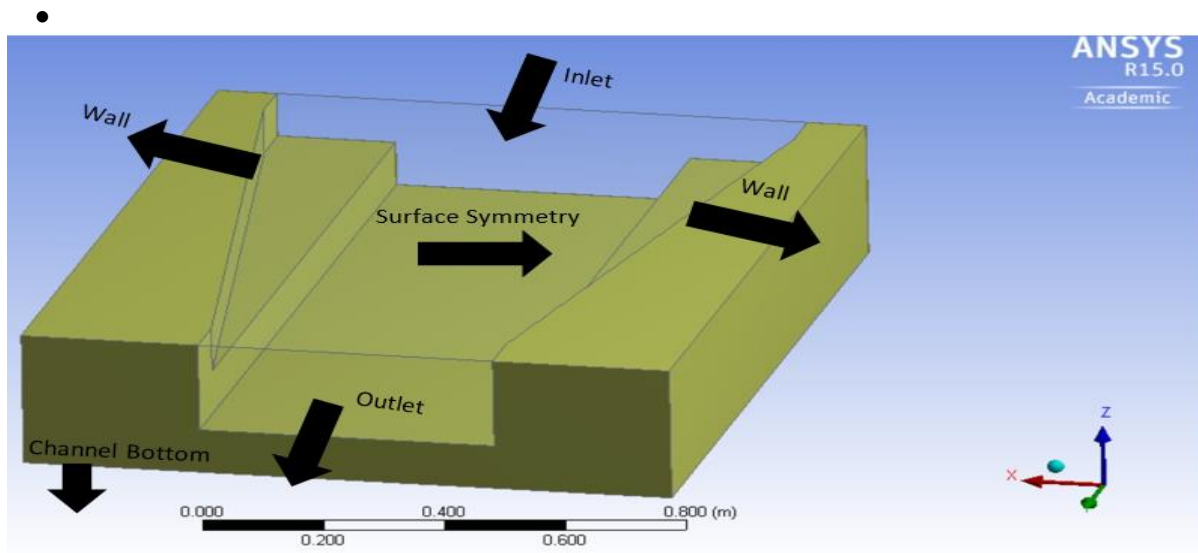


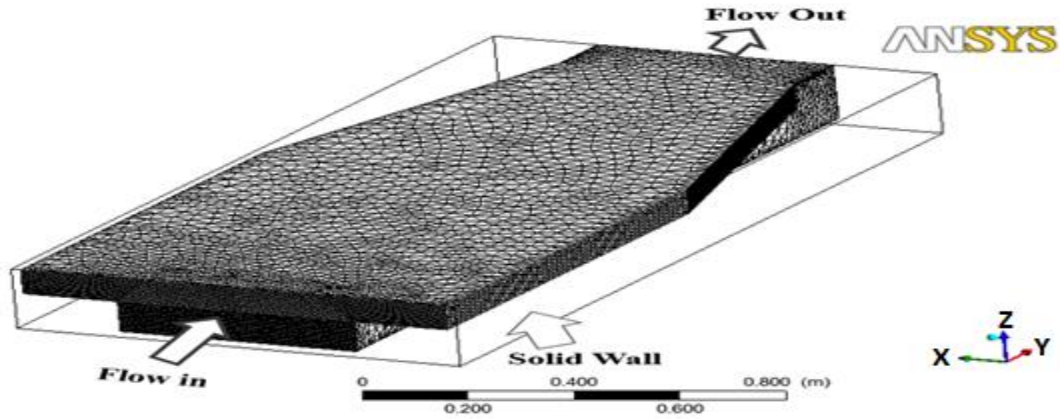
**Figure 1(c).** Typical grid showing the arrangement of velocity measurement points at the test sections (1-1,2-2,3-3,4-4 &5-5)



2. Geometry Setup of a Compound Channel with converging flood plains



3. Different Geometrical entities used in a compound channel with converging flood plain



4. A schematic view of the Grid used in the Numerical Model

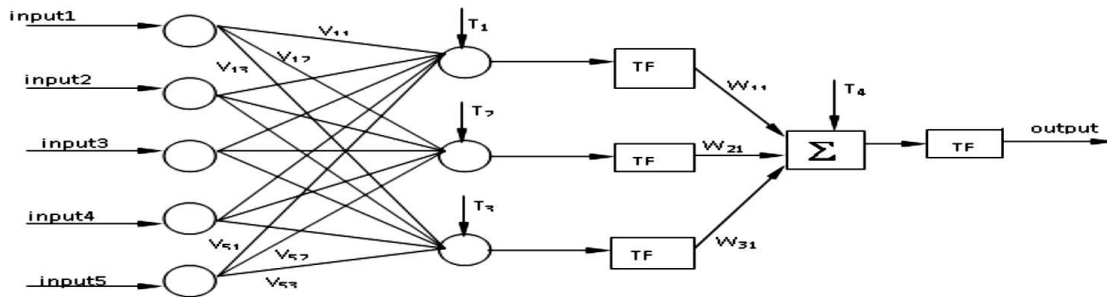
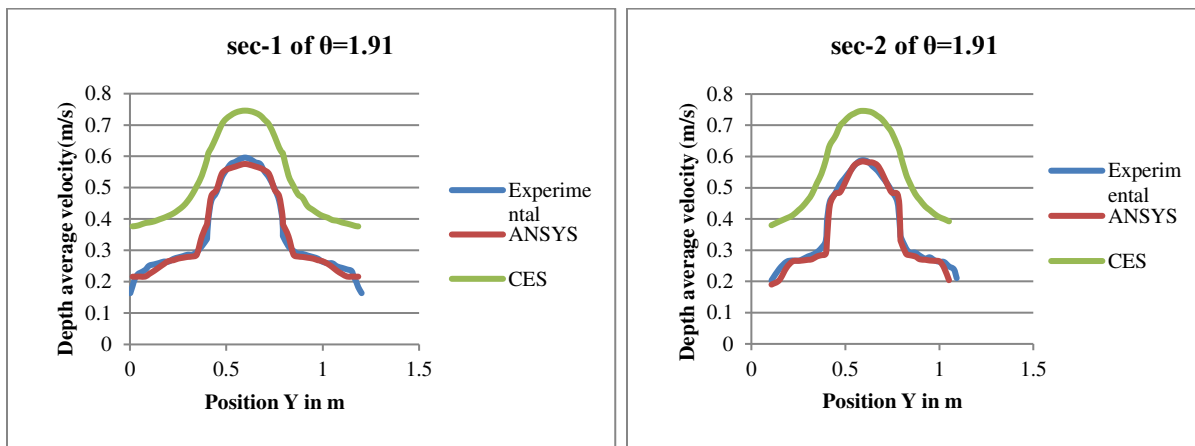
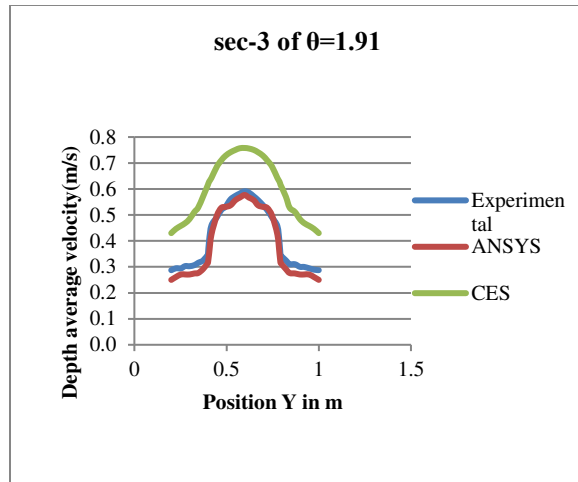
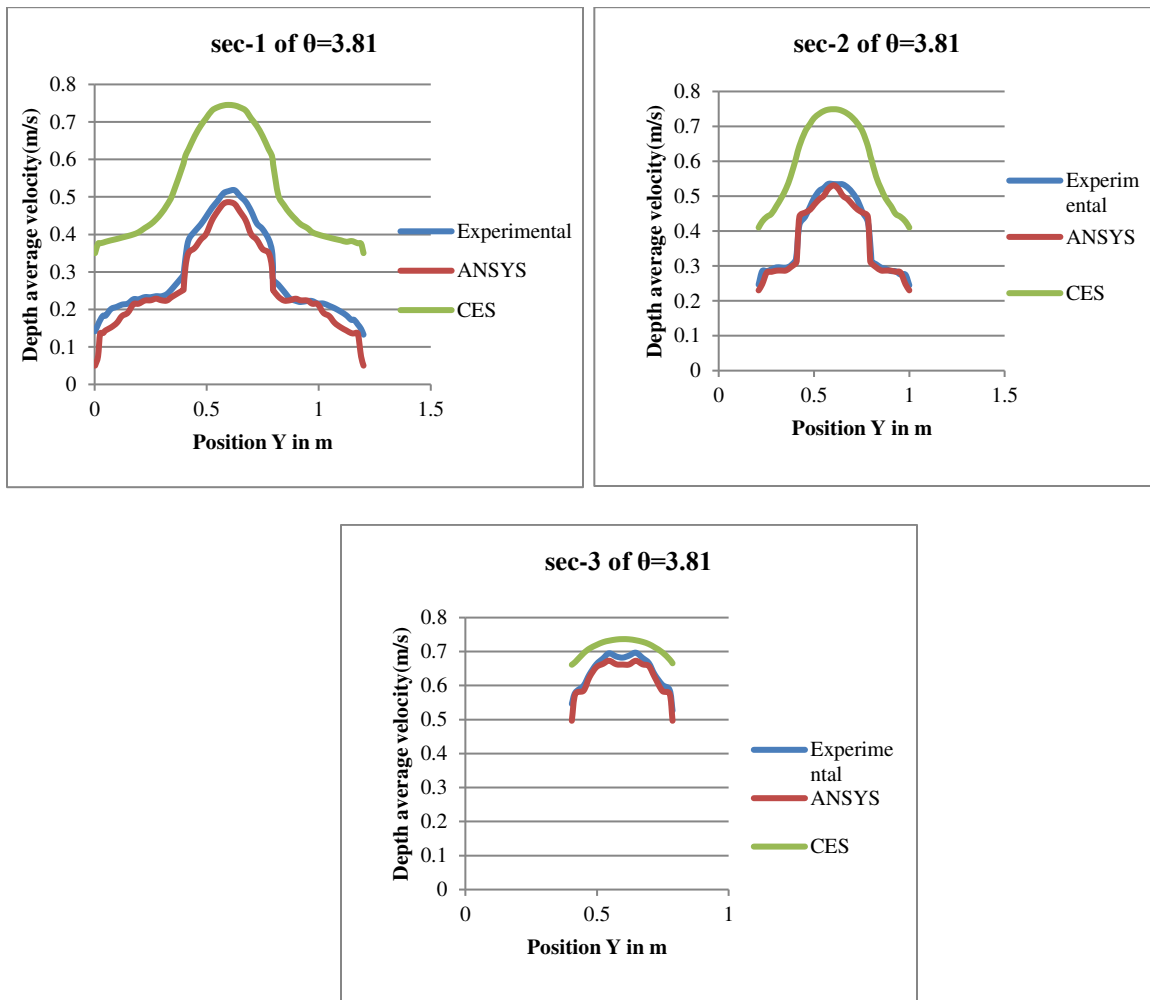


Fig.5. The architecture of back propagation neural network model





**Figure 6** (a) , (b) , (c) Depth-averaged velocity of Sec 1, Sec 2 , Sec 3 of  $\theta=1.91^{\circ}$



**Figure 7** (a) , (b) , (c) Depth-averaged velocity of Sec 1, Sec 2 , Sec 3 of  $\theta=3.81^{\circ}$

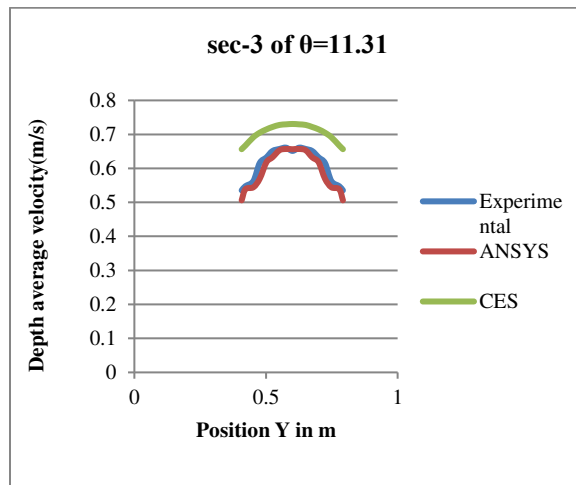
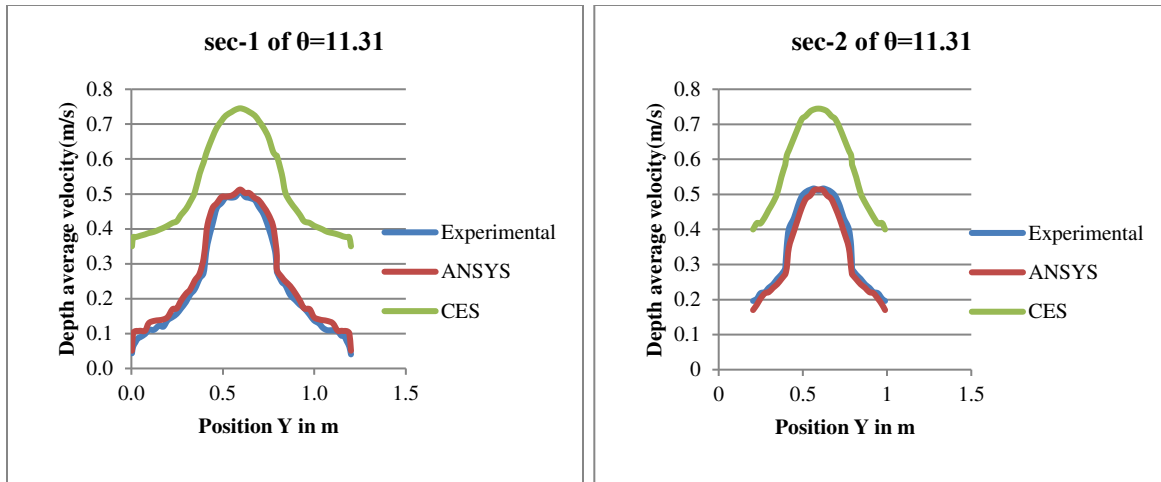
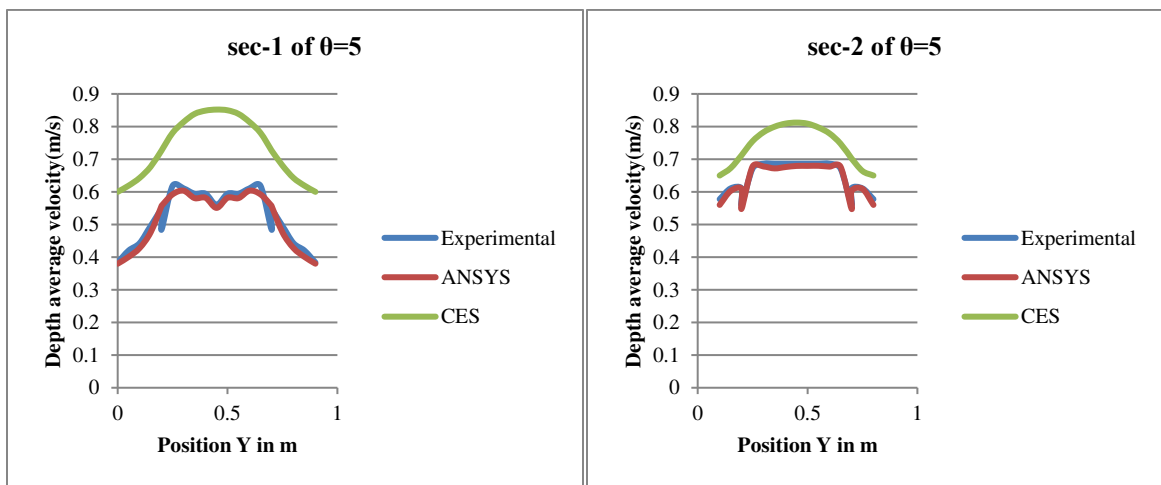
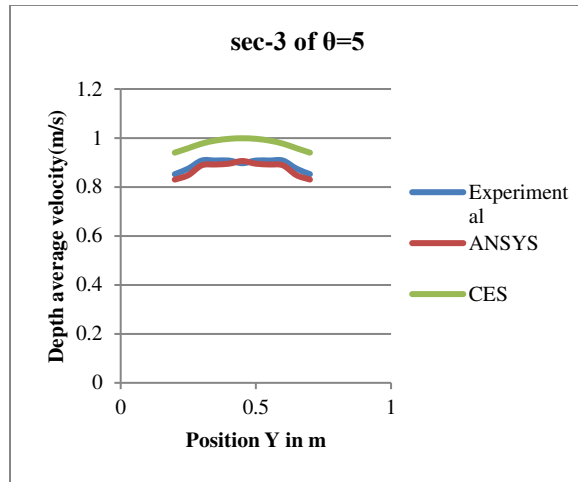
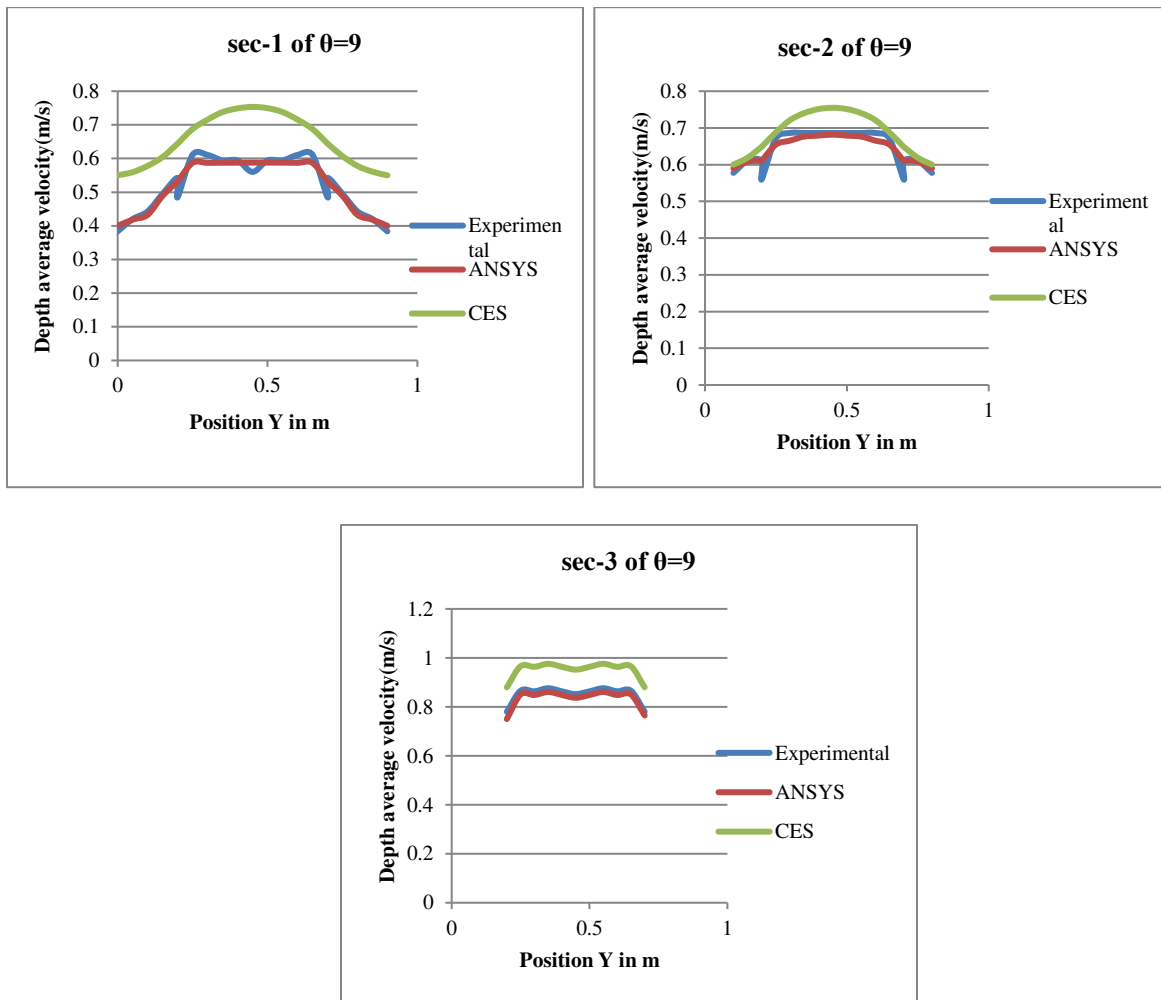


Figure 8 (a) , (b) , (c) Depth-averaged velocity of Sec 1, Sec 2 , Sec 3 of  $\theta=11.31^\circ$





**Figure 9** (a) , (b) , (c) Depth-averaged velocity of Sec 1, Sec 2 , Sec 3 of  $\theta =5^0$



**Figure 10** (a) , (b) , (c) Depth-averaged velocity of Sec 1, Sec 2 , Sec 3 of  $\theta =9^0$

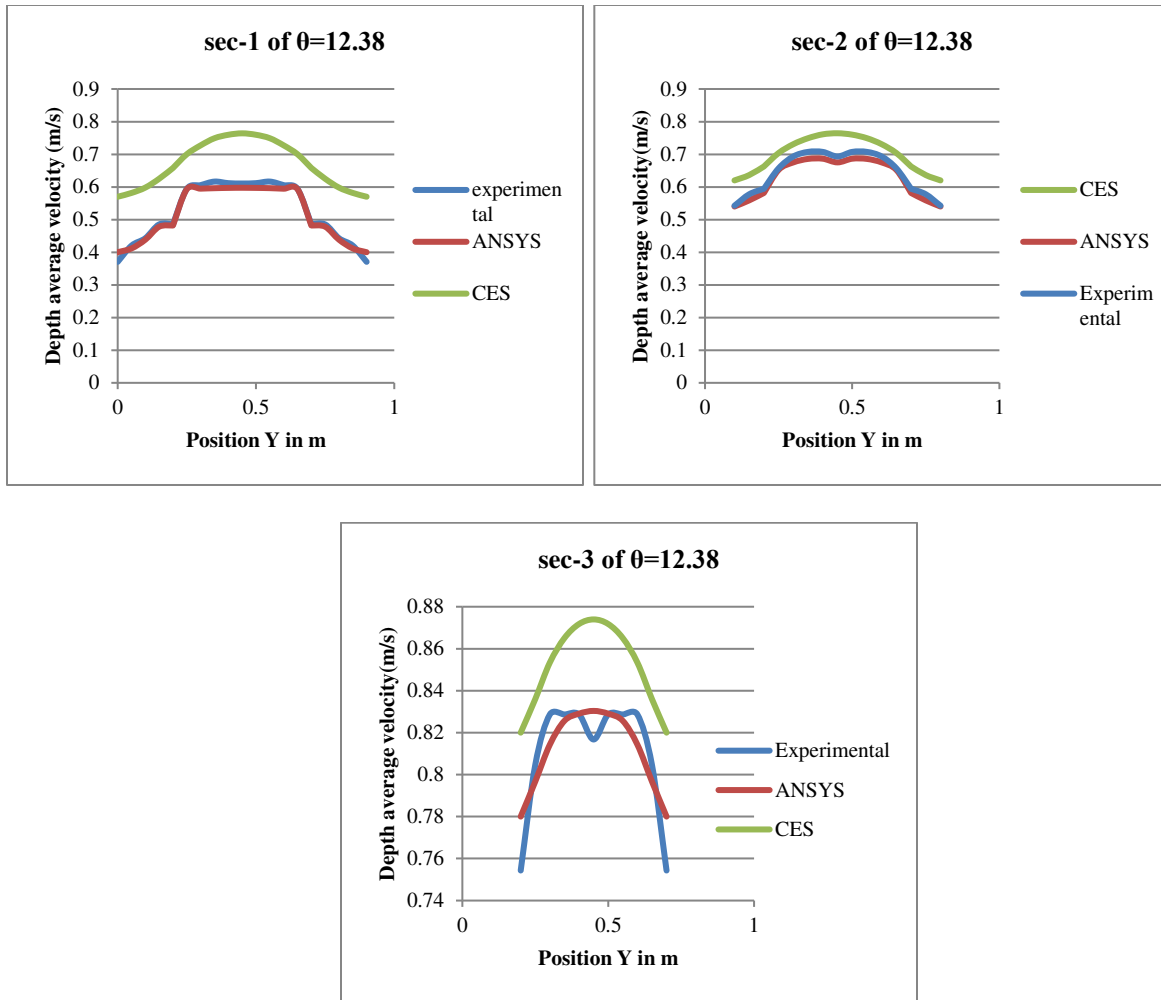


Figure 11 (a) , (b) , (c) Depth-averaged velocity of Sec 1, Sec 2 , Sec 3 of  $\theta = 12.38^\circ$

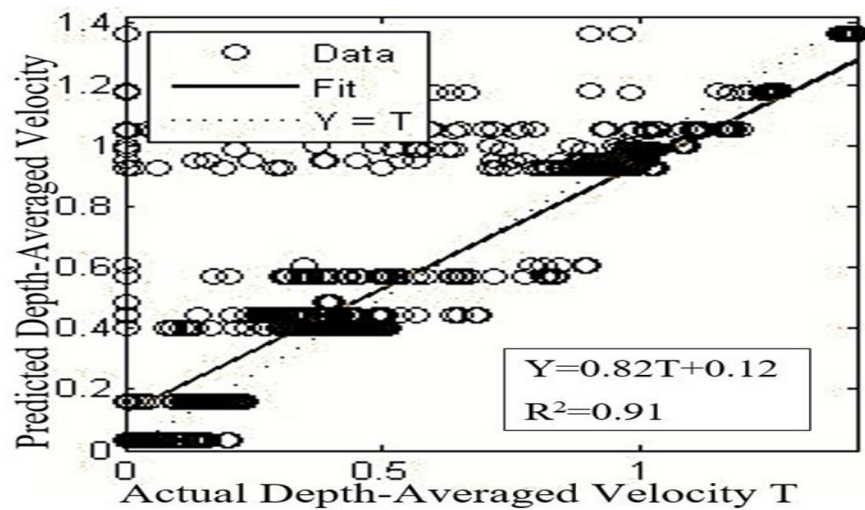
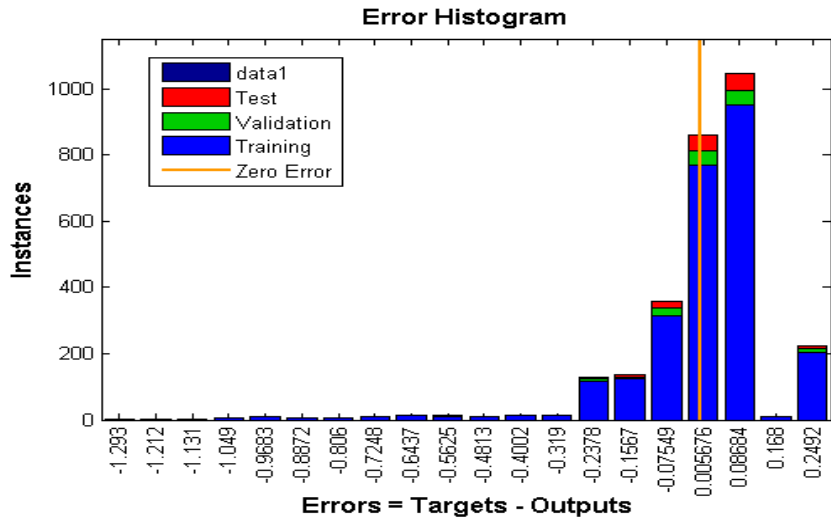


Fig 13 Correlation plot of actual depth-averaged velocity and predicted depth-averaged velocity



**Fig 14** Error Histogram